Wide InP Nanowires with Wurtzite/Zincblende Superlattice Segments Are Type-II whereas Narrower Nanowires Become Type-I: An Atomistic Pseudopotential Calculation

Lijun Zhang,[†] Jun-Wei Luo,[†] Alex Zunger,*,[†] Nika Akopian,[‡] Val Zwiller,[‡] and Jean-Christophe Harmand[¶]

[†]National Renewable Energy Laboratory, Golden, Colorado 80401, [‡]Kavli Institute of Nanoscience, Delft University of Technology, 2628 CJ Delft, The Netherlands, and [¶]CNRS-Laboratoire de Photonique et de Nanostructures, Route de Nozay, 91460 Marcoussis, France

ABSTRACT Nanowire-superlattices with different structural phases along the nanowire direction, such as wurtzite (WZ) and zincblende (ZB) forms of the same compound, often exhibit a "type II" band-alignment with electrons on ZB and holes on WZ. This is a material property of most of III−V semiconductors. We show via InP nanowires that as the nanowire diameter decreases, quantum-confinement alters this basic material property, placing both electrons and holes on the same (ZB) phase. This structural design causes a dramatic increase in absorption strength and reduced radiative lifetime.

KEYWORDS Electron-hole separation, nanowire superlattice, type II-type I transition

It has recently become possible to grow systems manifesting an interface between two structural polytypes of the same compound such as zincblende (ZB) and wurtzite (WZ).[1−10] Such interfaces usually have a calculated type II band alignment (such as SiC, GaN, GaAs, InP, InAs, CdTe, etc.),[11−13] where electrons and holes are spatially separated onto the different polytypes. For example a WZ/ZB homojunction of InP has electrons localized in ZB and holes from WZ.[12] Generally type II band alignment can be beneficial if one desires to dissociate electron−hole pairs (as in excitonic solar cells),[14] and can be detrimental if one wishes to have strong absorption with short radiative lifetimes (absorber devices).[15−17] Engineering such interfaces to realize a desired target electron−hole separation is thus relevant.

Type II offset was realized[3,5,6,8] in large-diameter (D) InP nanowires having various ZB segments with length L(ZB) along the [111] direction and WZ segments with length L(WZ) along the [0001] direction, as shown schematically in Figure 1. Atomistic pseudopotential calculations reported here, as well as the envelope function approximation model in ref 3 showed that no matter how short L(ZB) is, the first electron level e_0 is always bound in the ZB segment; similarly, no matter how short L(WZ) is, the first hole level h_0 is bound to the WZ segment (see Figure 2). Thus, formally, the system of wide (large D) wire superlattice is always type II irrespective of the lengths of the ZB and WZ segments along the wire direction. We show here via explicit atomistic

pseudopotential calculations how the absorption strength can nevertheless be significantly tuned by adjusting L(ZB) and L(WZ) even though the system persists as type II. This provides the straightforward explanation for the experimentally observed trend in radiative recombination lifetimes from the time-resolved photoluminescence data shown in Figure 4 below. More interestingly, we find that if the wire diameter D is reduced to below D_c = 7.5 nm then the hole level h_0 migrates into the ZB segment, whereas the electron level e_0 persists in the ZB segment, thus leading to a type I system. This finding is not yet examined experimentally as the current growth methods have not yet reached the capability of narrow WZ/ZB wires. Thus we offer this as a prediction. We predict that such narrow wires will convert the system to a strong absorber with shorter radiative lifetime, thus demonstrating engineering of type-I vs
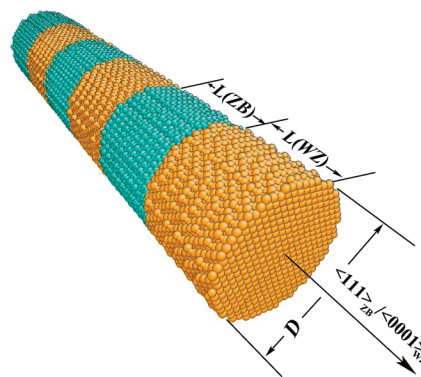

FIGURE 1. Schematic structure of the wurtzite/zincblende superlattice nanowire, defined with the wire diameter D and altering the ZB segment length L(ZB) and the WZ segment length L(WZ).

(a) ZB$_L$/WZ$_{50.8}$; Varying ZB segment; $D = \infty$

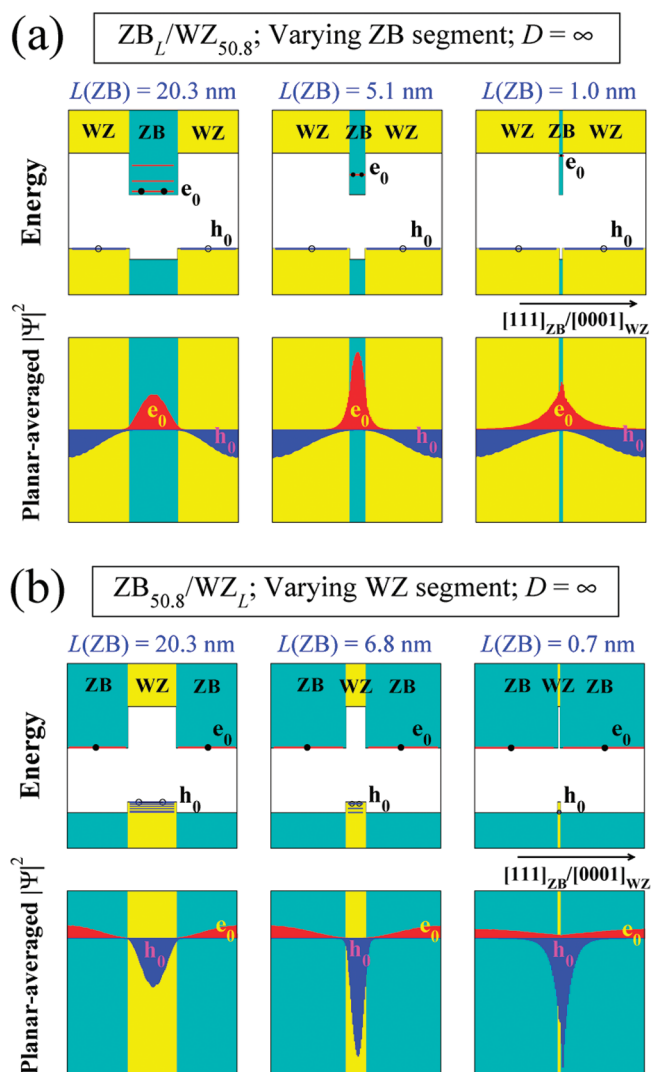## (b) ZB$_{50.8}$/WZ$_L$; Varying WZ segment; $D = \infty$

FIGURE 2. Single-particle energy and wave function square averaged in the superlattice plane for the first electron e_0 and the first hole h_0 in the ZB$_L$/WZ$_{50.8}$ (a) and ZB$_{50.8}$/WZ$_L$ (b) superlattice with the diameter $D = \infty$. Band edge alignment is based on calculated values for bulk ZB and WZ phases (Table 1), e.g., the WZ CBM is 112 meV higher than the ZB CBM and the WZ VBM is 29 meV higher than the ZB VBM. For the larger L(ZB) (L(WZ)), addtional electron (hole) states bound in ZB (WZ) segments are also shown.

type-II band alignment in the same material system via control of structure.

Method. We describe the nanosystem via solving the single-particle Schrödinger equation

$$\left[-\frac{\hbar^2}{2m}\nabla^2 + \sum_{n,\alpha} v_\alpha(\mathbf{r} - R_{n,\alpha}) + V_\alpha^{SO} \right]\psi_i(\mathbf{r}) = \varepsilon_i\psi_i(\mathbf{r})$$

(1)

where the wire potential is represented as a superposition of screened atomic pseudopotentials $v_\alpha(\mathbf{r} - R_{n,\alpha})$ centered at atom sites $R_{n,\alpha}$ (with includes nonlocal spin−orbit term

V_α^{SO}).[18] The screened pseudopotentials are fitted so as to reproduce the bulk band structure, effective masses, deformation potentials, and band alignment of InP in the ZB and WZ structures. Since there is no experimental data available on WZ InP except for the bandgap, we calculate these properties from the first-principle approach by using the transferability of the LDA potential from the ZB to WZ phase, for example, we first employ LDA+U[19] (and tune the value of U) to reproduce the experimental effective masses for the ZB phase, and then use the same U (and the transferable LDA potential) to calculate the effective masses of the WZ phase. The results on detailed pseudopotential fits are listed in Table 1. Eq 1 is solved by expanding the wave function in plane waves, evaluating all matrix elements numerically, and diagonalizing Hamiltonian via the folded spectrum method.[20,21] The WZ/ZB [0001]/[111] interface is generated by stacking In−P layers with the form of ABCABC for the ZB phase and then ABABAB for the WZ phase, making it atomically smooth.[4] At present, we employ the equilibrium structure for both ZB and WZ phase and do not consider the effect of strain and spontaneous polarization at the interface. Strain can exist in the WZ/ZB polytypic interfaces due to the difference in lattice constants of WZ and ZB phases. The difference is, however, slight (<0.5 % for InN and GaP) as the bond length mismatch is quite small.[22] This is a rather weak effect, indicated by the recent Raman spectroscopy study of WZ/ZB GaAs nanowires where the corresponding maximum spectral shift is only ∼4 cm^{-1}.[23] The spontaneous polarization charge for WZ InP has not been calculated before but is expected to have the smaller value than that of InN, ∼ −0.03 C/m^2.[24]

The optical absorption spectrum $I(E)$ is calculated, considering interband transitions, by using the dipole transition matrix $M_{v \to c} = \langle \Psi_v(\mathbf{r}) | \hat{p} | \Psi_c(\mathbf{r}) \rangle$

$$I(E) = \sum_c \sum_v |M_{v \to c}|^2 \exp\left[-\left(\frac{E - E_{vc}}{\sigma}\right)^2 \right]$$

(2)

that is, considering interband transitions, where $E_{vc} = E_c - E_v$ is the excitation energy and σ represents the spectral line broadening. The carrier radiative recombination lifetime (τ_{vc}) is calculated according to[25]

$$\frac{1}{\tau_{vc}} = \frac{4\alpha E_{vc} n |M_{v \to c}|^2}{m_0^2 \hbar c^2}$$

(3)

where n is the refractive index ($n = 3.5$ for photon energies around 1.5 eV in InP),[26] α is the fine-structure constant, m_0 is the electron rest mass, and c is the velocity of light.

Wide WZ/ZB Wires of InP Manifest Charge-Separation. When the wire diameter D is infinite, the system (Figure 1)

TABLE 1. Bulk Properties (Energies of VBM and CBM, Effective Masses, Deformation Potentials, etc.) from Present Empirical Pseudopotentials (EP) As Well As Those from Experiments and LDA + U (The Energy of CBM is Relative to That of VBM. Energies Are in eV and Effective Masses Are in m_0)

	ZB			WZ			
property	expt[a]	LDA+U	EP results	property	LDA+U	used target	EP results
$\varepsilon(\Gamma_{15v})$	−5.989[b]		−6.004	$\varepsilon(\Gamma_{5v})$		−5.975[c]	−5.975
$\varepsilon(\Gamma_{1c})$	1.424		1.425	$\varepsilon(\Gamma_{1c})$		1.504[d]/1.515[e]/1.508[f]	1.508
$m_e^*(\Gamma_{1c})$	0.077	0.064	0.059	$m_e^*(\Gamma_{1c})[1000]$	0.073	0.073	0.065
				$m_e^*(\Gamma_{1c})[0001]$	0.064	0.064	0.058
$m_{hh}^*[100]$	0.52	0.61	0.44	$m_{hh}^*[1000]$	0.14	0.14	0.13
$m_{hh}^*[111]$	0.95	1.24	1.18	$m_{hh}^*[0001]$	1.25	1.25	0.97
$m_{lh}^*[100]$	0.104	0.086	0.085	$m_{lh}^*[1000]$	0.18	0.18	0.17
				$m_{lh}^*[0001]$	0.16	0.16	0.12
$a(\Gamma)$	−6.4		−6.93				
$a_v(\Gamma)$	−0.41[g]		−0.68				
$b[100]$	−2.0		−1.67				
$\Delta_{so}(\Gamma)$	0.107	0.089	0.109	$\Delta_{so}(\Gamma)$	0.119	0.119	0.119
$\Delta_{so}(L)$	0.110	0.107	0.104	$\Delta_{cf}(\Gamma)$	0.026	0.026	0.026

[a] *Numerical Data and Functional Relationships in Science and Technology*; edited by Madelung, U., Schultz, M., Weiss, H., Eds.; Springer-Verlag, Berlin, 1997; Landolt Börnstein, New series, group III, Vol. 17a, 22a, 41a except where noted. [b] Wei, S. H.; Zunger, A. *Appl. Phys. Lett.* **1998**, *72*, 2011. [c] From our LDA calculations, the VBM of WZ is 0.029 meV higher than the VBM of ZB. [d] Mattila, M.; Hakkarainen, T.; Mulot, M.; Lipsanen, H. *Nanotechnology* **2006**, *17*, 1580. Here (also for the footnotes *e* and *f*) the bandgap difference between ZB and WZ phases is used to obtain WZ bandgap. [e] Ding, Y.; Motohisa, J.; Hua, B.; Hara, S.; Fukui, T. *Nano Lett.* **2007**, *7*, 3598. [f] Murayama, M.; Nakayama, T. *Phys. Rev.* B **1994**, *49*, 4710. [g] Wei, S. H.; Zunger, A. *Phys. Rev. B* **1999**, *60*, 5404.

becomes equivalent to a superlattice (SL) with altering the ZB and WZ segments along the SL direction. We consider both variation of L(ZB) at fixed (large) L(WZ) (Figure 2a) and variation of L(WZ) at fixed (large) L(ZB) (Figure 2b). In Figure 2a, it can be seen that the lowest electron level e_0 is bound in the ZB segment and the highest hole level h_0 is delocalized in the WZ segment. With decreasing ZB segment length L(ZB), the e_0 level gradually raises in energy (due to increased kinetic energy), approaching the conduction band minimum (CBM) of the bulk WZ phase (upper panels of Figure 2a), but the wave function stays spatially anchored to the ZB segment (lower panels of Figure 2a). This upward energy shift leads to a more spread-out e_0 wave function with increased leakage into WZ segments and thus leads to the increased overlap between e_0 and h_0 and to a stronger absorption and shorter radiative recombination lifetime (Figure 3a). Note that as L(ZB) gets wider, more electron states get bound in the ZB potential well (as in the L(ZB) = 20.3 nm case in upper panels of Figure 2a), which will contribute to additional peaks in the WZ (hole)-ZB (electron) indirect absorption (see Figure 3a).

Varying L(WZ) at fixed L(ZB) (Figure 2b) makes the e_0 level delocalized in the ZB segment and the h_0 level is bound in the WZ segment. With decreasing WZ period, the hole state moves deeper toward the ZB valence band maximum (VBM) (upper panels of Figure 2b), but stays anchored to the WZ segment (lower panels of Figure 2b). This h_0 level shift makes its wave function more spread-out, increasing the e_0-h_0 overlap and thus making the absorption stronger (see Figure 3b). (Note that for small L(WZ), the wave function peak of h_0 is obviously not well centered in WZ segments, which originates from the asymmetric potential shape formed by short WZ segments embedded in long ZB segments.)

Figure 3a,b shows the calculated absorption spectra and radiative lifetimes corresponding to Figure 2a,b, respectively. We include 10 electron states and one h_0 hole state for these calculations (the inclusion of more hole states only results in the broadening of absorption peaks). In Figure 3a, we see that with decreasing L(ZB), the h_0-e_0 absorption peak is blue shifted as the result of upward e_0 energy shift as mentioned above, and the absorption intensity increases reflecting enhanced leakage of e_0 from the ZB well (Figure 2a) and thus increased e_0-h_0 wave function overlap. In the L(ZB) = 10.2 nm case, a second electron bound state appears in the ZB segment, giving rise to an additional WZ (hole)−ZB (electron) absorption peak around 1.48−1.49 eV. Here the WZ (hole)−WZ (electron) direct absorption peak (in Figure 3a) is sightly blue shifted with respect to the value of the bulk WZ band gap (dash vertical line). This behavior is more remarkable in the smaller L(ZB) cases. Thus, it seems that ZB electrons somehow "repel" WZ electrons to higher energy when they overlap much.

The calculated carrier radiative lifetimes shown in Figure 3a are gradually reduced with decreasing L(ZB), due to the increased e_0-h_0 overlap. In particular, the lifetime for the WZ (hole)−WZ (electron) direct transition is 165 ps, which is independent of the change of L(ZB), whereas the WZ (hole)−ZB (electron) indirect recombination lifetime spans from 424 to 7947 ps for L(ZB) = 1.0 to 4.1 nm. Note that in the L(ZB) = 10.2 nm case, the additional absorption peak corresponding to the second ZB electron level also has shorter lifetime of 1324 ps. Turning to the spectra for varying L(WZ) with fixed wide L(ZB) in Figure 3b, the transition energy, absorption strength, and carrier lifetime of WZ (hole)−ZB (electron) indirect transitions are also clearly

(a)

Absorption spectrum: $ZB_L/WZ_{50.8}$; $D = \infty$

(b)

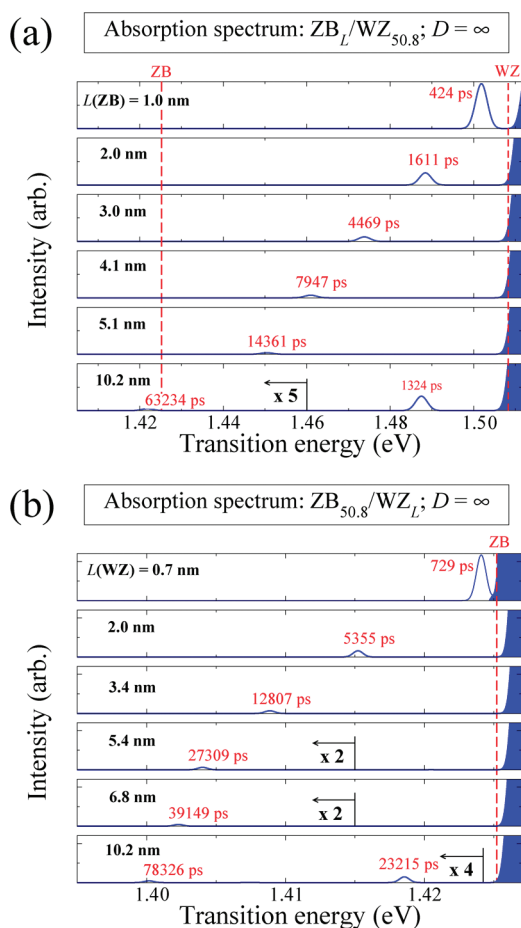Absorption spectrum: $ZB_{50.8}/WZ_L$; $D = \infty$

FIGURE 3. Absorption spectrum and radiative lifetime (marked onto individual peaks) for WZ (hole)-ZB (electron) indirect transitions in the $ZB_L/WZ_{50.8}$ (a) and $ZB_{50.8}/WZ_L$ (b) superlattice with the diameter $D = \infty$. The broadening of spectral lines is chosen as 2 and 0.5 meV for the $ZB_L/WZ_{50.8}$ and $ZB_{50.8}/WZ_L$, respectively. The energies corresponding to bulk ZB and WZ bandgaps are marked with vertical dash lines and shaded areas. Some weak peaks are enlarged to be visible.

FIGURE 4. (a) Time-resolved photoluminescence spectrum of a single WZ nanowire with short ZB sections. False-color plot represents time evolution of the PL after excitation by a laser pulse impinging at time 0. The upper part represents the PL intensity integrated over the full time window of 2 ns. The time evolutions of the PL peaks correspond to the cuts in the false-color plot, indicated by dashed lines and shown in the graph on the right with the corresponding colors. (b) Decay curves of the PL peaks in (a) measured in larger time window and plotted using the same color-code. The black solid lines represent monoexponential fits to the experimental data (for the blue and green curves) to obtain carrier lifetimes. The red curve (with the much longer lifetime) cannot be fitted with a single exponent.

tuned by the change of L(WZ), as expected from the results on single-particle energy and wave function in Figure 2b.

We turn to a direct comparison with the experiment. Figure 4 shows the time-resolved photoluminescence (PL) spectrum of a single wire with short ZB segments embedded in long WZ segments. The details of sample and experimental setup have been described in ref 8. The lengths of short ZB segments range from 1 monolayer to 10 monolayers (3 InP monolayers ~1.0 nm). As seen, the highest-energy spectral line of A (blue curve) among the observed ones, corresponding to the direct electron−hole recombination in the long WZ segments, shows a short lifetime of ~480 ps. This value is larger than the above calculated one, 165 ps, which might originate from the higher excitation power here leading to a bit overlapping of PL peaks. For lower excitation powers (in ref 8), there is less or even no overlapping and the measured lifetime is ~120 ps, which is in good agreement with the theoretical value. The lower-energy spe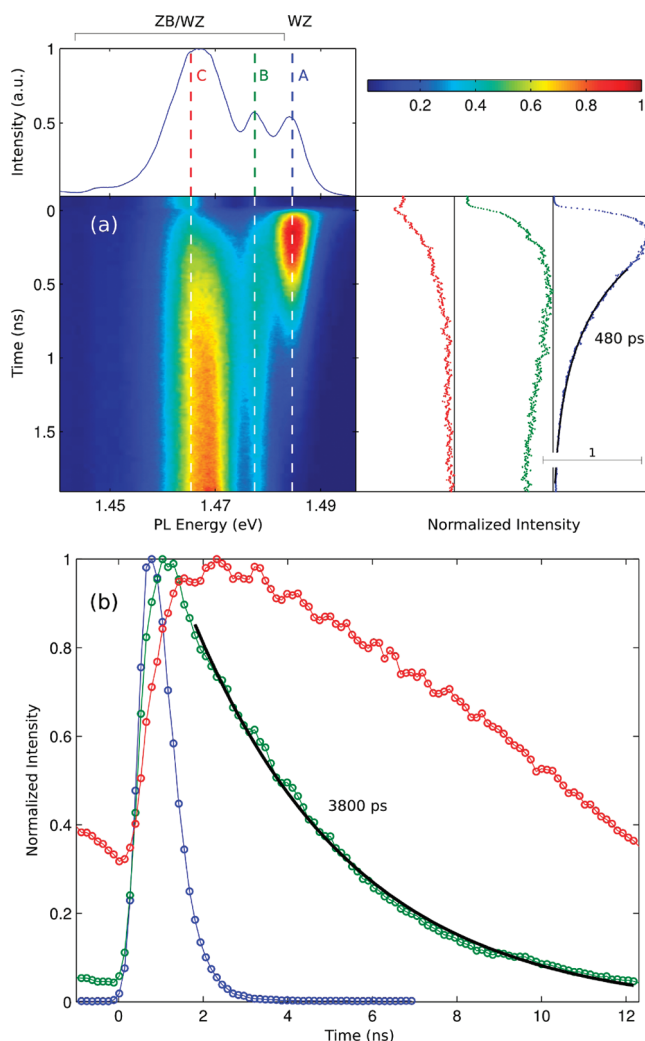ctral peaks, B (green curve) and C (red curve, consisting of several spectral lines) are attributed to recombination of electrons in short ZB segments having different length L(ZB) with holes in adjacent WZ segments. These WZ (hole)−ZB (electron) indirect transitions exhibit long lifetimes above 3800 ps. In addition, as the transition energy decreases (from A, and then B to C), the carrier lifetimes clearly show increasing trend. These behaviors are in good agreement with our theoretical results (Figure 3a), supporting the reliability of present calculations.

These results of Figure 2−3 for thick wires with $D = \infty$ stay essentially the same if the wire diameter is reduced to 10 nm, as shown in Figure 5 (Varying L(ZB) at fixed
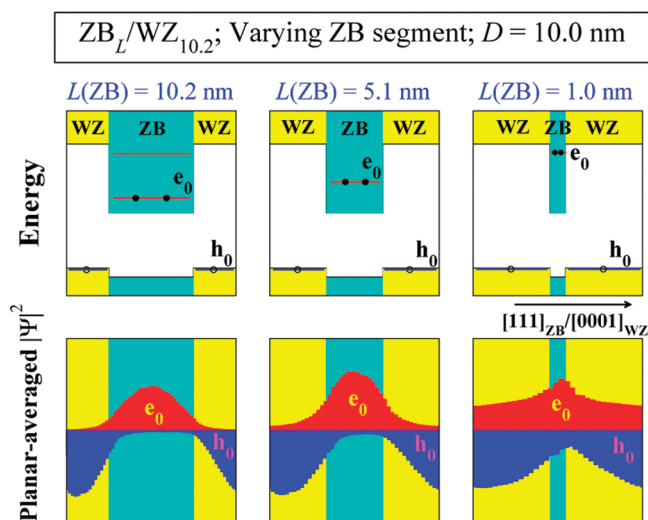
ZB$_L$/WZ$_{10.2}$; Varying ZB segment; D = 10.0 nm

FIGURE 5. Single-particle energy and planar-averaged wave function square for e$_0$ and h$_0$ in the ZB$_L$/WZ$_{10.2}$ wire with the 10 nm diameter. Here (and following Figure 6) band offsets are based on calculated band edges for pure ZB and WZ wires with the same diameter.
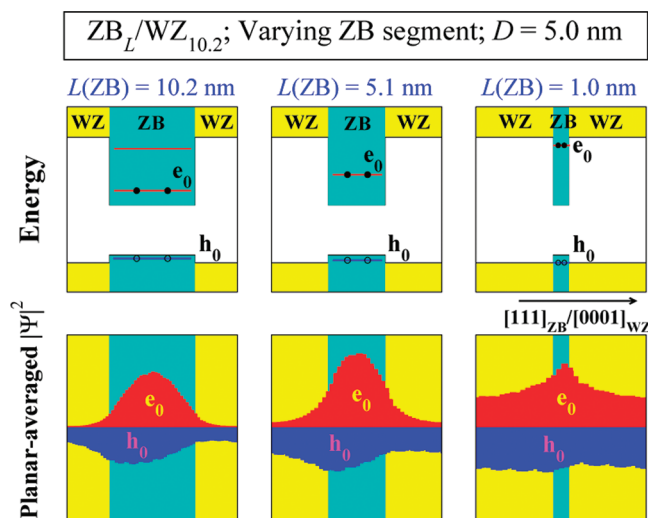
ZB$_L$/WZ$_{10.2}$; Varying ZB segment; D = 5.0 nm

FIGURE 6. Single-particle energy and planar-averaged wave function square for e$_0$ and h$_0$ in the ZB$_L$/WZ$_{10.2}$ wire with 5 nm diameter. Additional confined states bound in ZB segments are also shown. Note that the h$_0$ wave function is not symmetrically centered in the ZB section, which might result from the influence of the asymmetric WZ potential as mentioned since the confinement potential well of holes is shallow.

L(WZ) = 10.2 nm). However, when we continue reducing the wire diameter to 5 nm, we find a qualitative change as described next.

Narrow WZ/ZB Wires of InP Manifest a Type-I Alignment. Figure 6 shows the calculated single-particle energy and wave function of the lowest electron level e$_0$ and the highest hole level h$_0$ for varying L(ZB) at fixed L(WZ) = 10.2 nm in the wire with D = 5 nm. In contrast to above results, we find that h$_0$ is transferred from WZ segments into ZB segments, while e$_0$ stays bound in ZB segments. This forms a type I band alignment picture with both electrons and holes confined in the same material.

Some leakage of wave functions (even in the largest L(ZB) = 10.2 case) results from ZB segments not thick enough (the leakage is remarkably reduced for the calculation of ZB$_{20.3}$/WZ$_{20.3}$ with the same D) and the shallow potential well for holes. With decreasing ZB segments, the energies of both e$_0$ and h$_0$ are shifted toward the potential barriers (WZ band edges) and the penetration of their wave functions into WZ segments increases, consistent with the type I picture.

As a result of large overlap between e$_0$ and h$_0$ wave functions, which is a natural character for the type I system, the absorption spectra of the 5 nm wire show remarkably strong absorption strength of the h$_0$−e$_0$ transition. Its radiative lifetime is quite short, ∼150 ps. With decreasing L(ZB), its spectral line is blue shifted resulting from raised (both electrons and holes) energy levels in the potential wells by the increasing confinement in ZB segments.

The underlying physical mechanism of this structure-induced band-alignment transition in the nanoscale can be understood by considering the different properties of effective masses for the ZB and WZ phase. In the WZ phase there is a strong anisotropy of effective mass (m^*) for heavy hole (hh) states (dominating the VBM). This results in much smaller m^*(hh)$_{WZ}$ than m^*(hh)$_{ZB}$ in the wire confinement plane (e.g., the [011] direction for ZB and [1000] for WZ). As listed in Table 1, for the ZB phase m^*(hh)$_{ZB/[111]}$ = 1.18 and m^*(hh)$_{ZB/[011]}$ = 0.83, whereas in the WZ phase m^*(hh)$_{WZ/[0001]}$ = 0.97 and m^*(hh)$_{WZ/[1000]}$ = 0.13. The smaller m^*(hh)$_{WZ}$ in the confinement plane leads to stronger confinement for VBM of the WZ phase than that in the ZB phase. Then with decreasing wire diameter D in the type-II wide wires, quantum confinement makes the energy level of VBM(WZ) drop faster than that of VBM(ZB). This causes the formation of a cross between the energy evolutions of VBM(WZ) and VBM(ZB) with wire diameter at D_c = 7.5 nm. Below D_c, VBM(ZB) becomes the highest valence state and CBM(ZB) is still the lowest conduction state in the wire, thus converting the system to type I.

From the above analysis, the predicted type II to I transition in WZ/ZB wires is determined by two factors: (i) the anisotropy of effective mass for the heavy hole in the WZ phase, and (ii) the value of valence band offset between WZ and ZB phase. Recent band structure calculations by De and Pryor[27] reported similar anisotropy of effective mass for the heavy hole in most of III−V WZ semiconductors. It is to be mentioned that our results for the bulk InP WZ phase (in Table 1) differ in some cases from the results of Pryor et al.[27] These result from the different approach of constructing WZ pseudopotentials: our atomic WZ pseudopotentials, $v_\alpha(\mathbf{r} - R_{n,\alpha})$ and V_α^{SO} in eq 1, are fitted to reference calculations on the WZ structure, whereas Pryor et al. used directly ZB atomic potentials with some adjustments for WZ calculations (including the bandgap calculation). Our WZ bandgap value was fitted to experimental results[28,29] and previous theoreti-

cal result.[12] Despite not using the same methods, both calculations give similar results on the anisotropy of effective mass for the heavy hole in the WZ phase. As such, it can be conjectured that the type II to I transition might also occur in other WZ/ZB polytype systems. On the other hand, the larger valence band offset will lead to the occurrence of this transition (e.g., the cross of VBM(WZ) and VBM(ZB)) at narrower wires. For example in GaAs, the calculated valence band offset is 84 meV, which is about two times larger than that of InP (45 meV) using the same approach.[12] Thus, quite thin wires might be required to observe this structure-induced type II to I transition.

REFERENCES AND NOTES

(1) Jacobs, B.; Ayres, V.; Petkov, M.; Halpern, J.; He, M.; Baczewski, A.; McElroy, K.; Crimp, M.; Zhang, J.; Shaw, H. *Nano Lett.* **2007**, *7*, 1435–1438.

(2) Algra, R.; Verheijen, M.; Borgstrm, M.; Feiner, L.; Immink, G.; van Enckevort, W.; Vlieg, E.; Bakkers, E. *Nature* **2008**, *456*, 369–372.

(3) Bao, J.; Bell, D.; Capasso, F.; Wagner, J.; Mårtensson, T.; Trgårdh, J.; Samuelson, L. *Nano Lett.* **2008**, *8*, 836–841.

(4) Caroff, P.; Dick, K. A.; Johansson, J.; Messing, M. E.; Deppert, K.; Samuelson, L. *Nat. Nanotechnol.* **2009**, *4*, 50–55.

(5) Spirkoska, D.; Arbiol, J.; Gustafsson, A.; Conesa-Boj, S.; Glas, F.; Zardo, I.; Heigoldt, M.; Gass, M. H.; Bleloch, A. L.; Estrade, S.; Kaniber, M.; Rossler, J.; Peiro, F.; Morante, J. R.; Abstreiter, G.; Samuelson, L.; Fontcuberta i Morral, A. *Phys. Rev. B* **2009**, *80*, 245325.

(6) Pemasiri, K.; Montazeri, M.; Gass, R.; Smith, L.; Jackson, H.; Yarrison-Rice, J.; Paiman, S.; Gao, Q.; Tan, H.; Jagadish, C.; Zhang, X.; Zou, J. *Nano Lett.* **2009**, *9*, 648–654.

(7) Hoang, T.; Moses, A.; Zhou, H.; Dheeraj, D.; Fimland, B.; Weman, H. *Appl. Phys. Lett.* **2009**, *94*, 133105.

(8) Akopian, N.; Patriarche, G.; Liu, L.; Harmand, J.; Zwiller, V. *Nano Lett.* **2010**, *10*, 369–372.

(9) Smith, L. M.; Jackson, H. E.; Yarrison-Rice, J. M.; Jagadish, C. *Semicond. Sci. Technol.* **2010**, *25*, No. 024010.

(10) Fissel, A.; Schrter, B.; Kaiser, U.; Richter, W. *Appl. Phys. Lett.* **2000**, *77*, 2418.

(11) Wei, S.-H.; Zhang, S. B. *Phys. Rev. B* **2000**, *62*, 6944–6947.

(12) Murayama, M.; Nakayama, T. *Phys. Rev. B* **1994**, *49*, 4710–4724.

(13) Bechstedt, F.; Kckell, P. *Phys. Rev. Lett.* **1995**, *75*, 2180–2183.

(14) Gregg, B. *J. Phys. Chem. B* **2003**, *107*, 4688–4698.

(15) Mikhailova, M.; Titkov, A. *Semicond. Sci. Technol.* **1994**, *9*, 1279–1295.

(16) Baier, T.; Mantz, U.; Thonke, K.; Sauer, R.; Schffler, F.; Herzog, H.-J. *Phys. Rev. B* **1994**, *50*, 15191–15196.

(17) Liu, Q.; Derksen, S.; Linder, A.; Scheffer, F.; Prost, W.; Tegude, F. *J. Appl. Phys.* **1995**, *77*, 1154–1158.

(18) Zunger, A. In *Quantum Theory of Real Materials*; Kluwer: Boston, 1996.

(19) Liechtenstein, A. I.; Anisimov, V. I.; Zaanen, J. *Phys. Rev. B* **1995**, *52*, R5467–R5470.

(20) Wang, L.; Zunger, A. *J. Chem. Phys.* **1994**, *100*, 2394.

(21) Wang, L. W.; Zunger, A. In *Semiconductor Nanoclusters*; Elsevier: New York, 1996.

(22) Yeh, C.-Y.; Lu, Z. W.; Froyen, S.; Zunger, A. *Phys. Rev. B* **1992**, *46*, 10086–10097.

(23) Zardo, I.; Conesa-Boj, S.; Peiro, F.; Morante, J. R.; Arbiol, J.; Uccelli, E.; Abstreiter, G.; Fontcuberta i Morral, A. *Phys. Rev. B* **2009**, *80*, 245324.

(24) Bernardini, F.; Fiorentini, V.; Vanderbilt, D. *Phys. Rev. B* **1997**, *56*, R10024–R10027.

(25) Dexter, D. L. *Solid State Physics*; Academic Press: New York, 1958.

(26) *Semiconductors: Group IV Elements, IV-IV and III-V Compunds*; Rössler, U., Ed.; Springer-Verlag, Berlin, 2001; Landolt-Börnstein, New Series, Group III, Vol. 41, Pt. a.

(27) De, A.; Pryor, C. E. *Phys. Rev. B* **2010**, *81*, 155210.

(28) Mattila, M.; Hakkarainen, T.; Mulot, M.; Lipsanen, H. *Nanotechnology* **2006**, *17*, 1580.

(29) Ding, Y.; Motohisa, J.; Hua, B.; Hara, S.; Fukui, T. *Nano Lett.* **2007**, *7*, 3598–3602.